

Dendritic Branching Angles of Pyramidal Cells Across Layers of the Juvenile Rat Somatosensory Cortex

Ignacio Leguey,^{1*} Concha Bielza,¹ Pedro Larrañaga,¹ Asta Kastanauskaite,² Concepción Rojo,^{2,3} Ruth Benavides-Piccione,^{2,4} and Javier DeFelipe^{2,4}

¹Departamento de Inteligencia Artificial, Escuela Técnica Superior de Ingenieros Informáticos, Universidad Politécnica de Madrid, Madrid, Spain

²Laboratorio Cajal de Circuitos Corticales, Centro de Tecnología Biomédica, Universidad Politécnica de Madrid, Madrid, Spain

³Departamento de Anatomía y Anatomía Patológica Comparada, Facultad de Veterinaria, Universidad Complutense de Madrid, Madrid, Spain

⁴Instituto Cajal, Consejo Superior de Investigaciones Científicas, Madrid, Spain

The characterization of the structural design of cortical microcircuits is essential for understanding how they contribute to function in both health and disease. Since pyramidal neurons represent the most abundant neuronal type and their dendritic spines constitute the major postsynaptic elements of cortical excitatory synapses, our understanding of the synaptic organization of the neocortex largely depends on the available knowledge regarding the structure of pyramidal cells. Previous studies have identified several apparently common rules in dendritic geometry. We study the dendritic branching

angles of pyramidal cells across layers to further shed light on the principles that determine the geometric shapes of these cells. We find that the dendritic branching angles of pyramidal cells from layers II–VI of the juvenile rat somatosensory cortex suggest common design principles, despite the particular morphological and functional features that are characteristic of pyramidal cells in each cortical layer. *J. Comp. Neurol.* 524:2567–2576, 2016.

© 2016 Wiley Periodicals, Inc.

INDEXING TERMS: neuronal geometrical design; Jones-Pewsey and von Mises directional statistics; branching dendritic angles; cortical layers; nif-0000-10474; nif-0000-10294; RGD_5508396

Pyramidal neurons represent the most abundant neuronal type in the cerebral cortex. Their dendritic spines constitute the major postsynaptic elements of cortical excitatory synapses and are fundamental to memory, learning, and cognition (Spruston, 2008; Yuste, 2010; DeFelipe, 2015). Thus, our understanding of the synaptic organization of the neocortex largely depends on the available knowledge regarding pyramidal cells.

To date, several studies have shown that pyramidal cells sampled from different areas of different species, including rodents and primates, present quantitative differences in the size and complexity of the dendritic arbor and the density of spines (Elston et al., 2001; Jacobs et al., 2001; Elston, 2003; Benavides-Piccione et al., 2006). Also, differences between layers and age have been reported in various species (Larkman, 1991; Petanjek et al., 2008; Oberlander et al., 2012; Benavides-Piccione et al., 2012). These variations reflect differences in cortical information processing. For example, different branch structures are responsible

for different forms of processing within the dendritic tree before input potentials arrive at the soma (reviewed in Stuart and Spruston, 2015). Therefore, there may be a greater potential for compartmentalization in areas that contain highly branched pyramidal

Supporting information may be found at <http://cig.fi.upm.es/suppmaterial/Legueyetal>.

Grant sponsor: Spanish Ministry of Economy and Competitiveness through the Cajal Blue Brain (C080020-09; the Spanish partner of the Blue Brain initiative from EPFL); Grant sponsor: TIN2013-41592-P projects, by the Regional Government of Madrid through the S2013/ICE-2845-CASI-CAM-CM project; Grant sponsor: European Union's Seventh Framework Programme (FP7/2007-2013); Grant number: 604102 (Human Brain Project); Grant sponsor: Spanish Ministry of Education, Culture and Sport Fellowship; Grant number: FPU13/01941 (to I.L.).

*CORRESPONDENCE TO: Ignacio Leguey, Departamento de Inteligencia Artificial, Escuela Técnica Superior de Ingenieros Informáticos, Universidad Politécnica de Madrid (UPM), Campus Montegancedo s/n, Pozuelo de Alarcón, 28223 Madrid, Spain. E-mail: ig.leguey@upm.es

Received September 4, 2015; Revised February 1, 2016; Accepted February 2, 2016.

DOI 10.1002/cne.23977

Published online February 18, 2016 in Wiley Online Library (wileyonlinelibrary.com)

© 2016 Wiley Periodicals, Inc.

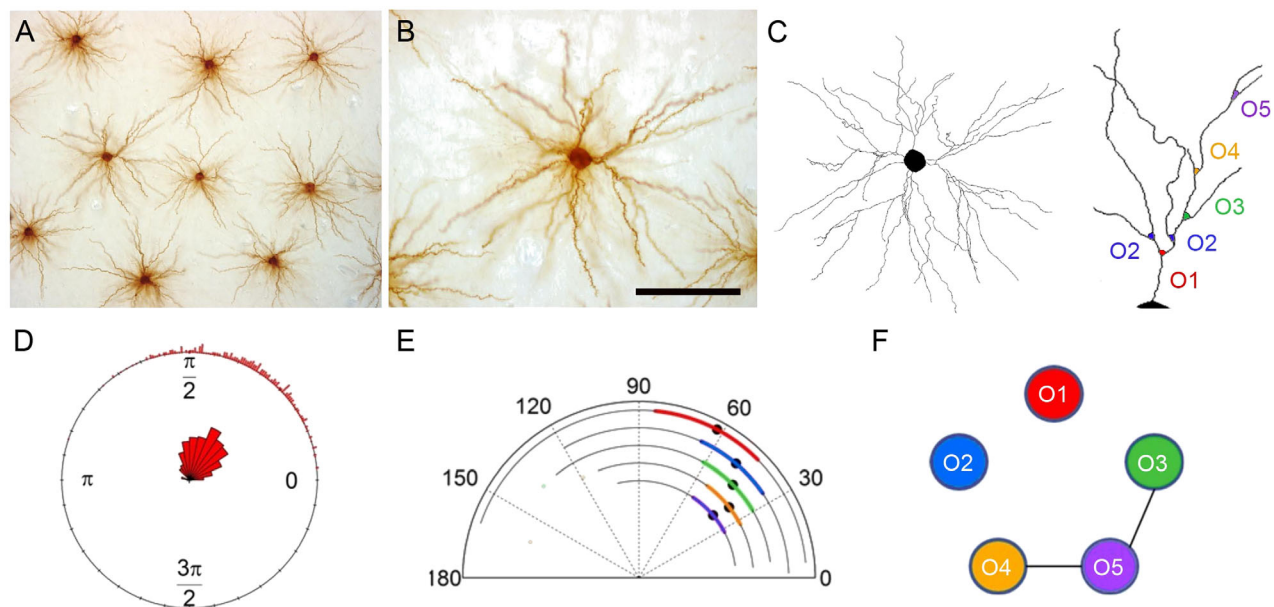


Figure 1. **A:** Low-power photomicrograph showing injected neurons in layers III from the S1HL region of P14 rats, as seen in the plane of section parallel to the cortical surface. **B:** Higher-magnification photomicrograph showing an example of a pyramidal cell basal dendritic arbor. **C:** Schematic drawing of the basal arbor of the pyramidal neuron shown in B. Angles of different branch orders (shown on the right in different colors) were measured between sibling segments. **D:** Example of a rose diagram overlapped with a circular histogram of the distribution of branching angles (in degrees) of the same branch order 1 in layer II. **E:** Circular boxplot of the angles showing the summary statistics of a dataset as arcs inside a semicircle. The black dot is the median direction, the colored lines are the boxes (from the lower quartile (Q1) to the upper quartile (Q3)), the black lines are the whiskers that depend on the interquartile range (Q3-Q1) and the concentration parameter (κ) of the distribution, and the colored dots are the outliers that do not belong to the box-and-whiskers interval. The respective graphs correspond to the comparison between different branch order angles in layer II. **F:** Test-based diagram illustrating the pairwise comparisons of the mean angles from datasets shown in D. Two nodes (each node is a dataset) between which there is no statistically significant difference are connected, meaning that the null hypothesis of the Watson nonparametric test cannot be rejected. Scale bar = 200 μm for A; 90 μm for B.

cells than in areas with less branched cells (reviewed in Elston, 2003).

Previous studies have identified several rules that seem to be common in dendritic geometry. For example, it has been proposed that geometric theory predicts bifurcations in minimal wiring cost trees (Cuntz et al., 2008, 2010, 2012; Wen et al., 2009; van Pelt and Uylings, 2011; Kim et al., 2012). Also, it has been described that dendrites usually branch when they are close to the soma to produce short segments, whereas the segments that do not branch spread away from the soma (Samsonovich and Ascoli, 2003; López-Cruz et al., 2011). These studies have shown that segment orientation is mainly controlled by the orientation of the previous segments and that dendritic trees tend to first spread rapidly when they are close to the soma and then, once they have reached a minimum size, grow straight away from the soma. Additionally, the first bifurcation of a particular basal tree is the widest, and subsequent bifurcations become progressively narrower (López-Cruz et al., 2011; Bielza et al., 2014). Moreover, the final bifurcation of a particular cortical region is

rather similar, regardless of the branch order of the dendrite (Bielza et al., 2014).

We analyzed the geometry of pyramidal cell basal arbors in different cortical layers of the juvenile Wistar rat (RRID: RGD_5508396) somatosensory cortex to determine if the above rules are applicable to the different cortical layers. We used Wistar rats at postnatal day 14 since we intended to integrate these data with other anatomical, molecular, and physiological data that have already been collected from the same cortical region of the P14 Wistar rats. The final goal is to create a detailed, biologically accurate model of circuitry through layers 2–6 in the primary somatosensory cortex, within the framework of the Blue Brain Project (<http://bluebrain.epfl.ch/>). We found that the first bifurcation of a particular basal tree is the widest, and subsequent bifurcations become progressively narrower in all analyzed cortical layers. Also, the final bifurcation angle of a dendritic tree is similar, regardless of its complexity. In addition, angles of the same branch order are similar to each other across the different cortical layers.

MATERIALS AND METHODS

Data

A set of 288 3D pyramidal neurons from six different layers of the 14-day-old (P14) rat hind limb somatosensory (S1HL) neocortex was used for the analysis. Current methodological limitations restrict us to the study of either the complete basal arbors (horizontal sections) or truncated apical and basal arbors (coronal sections). For the sake of consistency with our previous studies, we opted to study the basal dendrites. Thus, pyramidal neurons were intracellularly injected in horizontal sections to allow the study of complete basal dendritic arbors. Briefly, cells in layers II, III, IV, Va, Vb, and VI were individually injected with Lucifer Yellow, which was applied by continuous current until the distal tips of each dendrite fluoresced brightly. Following injections, the sections were processed with an antibody to Lucifer Yellow to visualize the complete morphology of the cells (Fig. 1A,B). Only neurons that had an unambiguous apical dendrite and whose basal dendritic tree was completely filled and contained within the section were included in the analysis (48 cells from each layer; six cells per layer, six layers, eight animals). The NeuroLucida package (MicroBrightField, Williston, VT; <http://www.mbfioscience.com/neuroLucida>. RRID: nif-0000-10294, SCR_001775) was used to three-dimensionally trace the basal dendritic arbor of each pyramidal cell (Fig. 1C). Reconstruction of the same neurons has been used previously in another study for different purposes (Rojo et al., 2016). Further information regarding tissue preparation, injection methodology, immunohistochemistry processing, and 3D reconstruction is outlined in Rojo et al. (2016).

In the present study we measured the angle between two sibling segments originating from a bifurcation of the basal dendritic trees (Fig. 1A). Given a bifurcation point O with coordinates (x_0, y_0, z_0) and two points $A = (x_1, y_1, z_1)$ and (x_2, y_2, z_2) defining the endpoints of the segments growing from the bifurcation, the angle ϕ between the vectors OA and OB is given by:

$$\phi = \arccos\left(\frac{OA \cdot OB}{\|OA\| \|OB\|}\right) \quad (1)$$

where \cdot represents the scalar product of the vectors and $\|u\|$ is the magnitude of the vector u .

The above angles were grouped based on the number of bifurcations that take place in the path that starts at the soma and ends at the angle, meaning that the first bifurcation that takes place in a dendritic arbor would be "Order 1" (denoted by O1), the next possible bifurcations would be "Order 2" (O2), etc. Branch order angles greater than O5 were not included in the

analysis due to the relatively low number (Supplementary Table S1).

Directional statistics

Directional statistics (Fisher, 1993; Mardia and Jupp, 1999; Jammalamadaka and SenGupta, 2001) have to be used to properly manage this kind of data. Directional statistics differ from traditional statistics with respect to some special properties such as periodicity and the representation of points on the circumference of the unit circle (instead of the real line for linear data).

The von Mises distribution

The von Mises (vM) distribution (von Mises, 1918) is the directional analog of the Gaussian distribution and is the most commonly used distribution in directional statistics. The vM distribution of a random variable is a two-parameter distribution with the probability density function:

$$f(x, \mu, \kappa) = \frac{1}{2\pi I_0(\kappa)} \exp(\kappa \cos(x - \mu)), \quad (2)$$

where the domain is the unit circle, which define angles $x \in [0, 2\pi]$, μ is the mean direction of X , $\kappa \geq 0$ is the concentration of the angles around the mean and I_0 is the Bessel function of the first kind of order 0:

$$I_0(\kappa) = \frac{1}{2\pi} \int_0^{2\pi} \exp(\kappa \cos x) dx \quad (3)$$

The vM density is unimodal and symmetric around the mean direction; the density is uniform when $\kappa = 0$, whereas high values of κ yield points that are tightly clustered around μ .

Maximum likelihood estimator of μ is the sample mean direction, while maximum likelihood estimator of κ cannot be computed analytically and numerical approximations have to be used (Fisher, 1993; Mardia and Jupp, 1999).

The Jones-Pewsey distribution

The Jones-Pewsey (JP) distribution (Jones and Pewsey, 2005) is a broader three-parameter family of symmetric circular distributions. The probability density function is:

$$f(x, \mu, \kappa, \psi) = \frac{\{\cosh(\kappa\psi) + \sinh(\kappa\psi)\cos(x - \mu)\}^{1/\psi}}{2\pi P_{1/\psi}(\cosh(\kappa\psi))} \quad (4)$$

where the x domain is $[0, 2\pi]$, μ is the location parameter, $\kappa \geq 0$ is the concentration parameter akin to that of the vM distribution, $-\infty < \psi < \infty$ is the shape, and $P_{1/\psi}$ is the associated Legendre function of the first kind of degree $1/\psi$ and order 0 (Gradshteyn and Ryzhik, 1994; Zwillinger, 1997).

Several circular models are obtained from the JP distribution, including the vM distribution when $\psi = 0$.

Graphs

In this study we used rose diagrams, circular histograms, and circular boxplots to plot the data.

Rose diagrams and circular histograms

In the rose diagram we divided the circumference into sectors with the same arc length, and the area of each sector reveals the number of angles that it contains. We also plotted the corresponding circular histogram for each rose diagram (Fig. 1D).

Circular boxplots

We used the recently developed circular boxplot (Fig. 1E) (Abuzaid et al., 2012):

- Black dots are the median directions, calculated as the value of the sample that minimizes the sum of circular distances (Fisher, 1993).
- Colored lines are the boxes that represent the interquartile range (CIQR), calculated as upper quartile - lower quartile, that is, $CIQR = Q3 - Q1$.
- Black lines are the whiskers, whose length depends on the CIQR and the resistant constant (v), which in turn depends on the concentration κ of the sample:
 - Lower whisker limit: $Q1 + v * CIQR$
 - Upper whisker limit: $Q3 - v * CIQR$

$$v = \begin{cases} 1.5, & 2 \leq \kappa < 3 \\ 2.5, & \kappa > 3 \end{cases}$$

The resistant constant changes with the concentration in order to ensure that an overlapping of the lower and upper fences does not occur. For $\kappa < 2$, it is difficult to find a circular boxplot with nonoverlapping fences, as the data are close to being uniform.

- Colored dots outside the whiskers are the outliers.

This kind of chart is useful for plotting different boxplots on the same figure for the purpose of comparison. Due to the range of the angles output in the study, the boxplot is represented as a 180° semicircle instead of as a full 360° circle.

Statistical tests

We used the following statistical tests.

Goodness-of-fit

In order to test the goodness-of-fit to a vM distribution, we used the Watson U^2 test adaptation for the vM distribution (Lockhart and Stephens, 1985) at a

significance level of $\alpha = 0.05$ (Supplementary Tables S2–S3).

In the case of the JP distribution, we tested the goodness-of-fit using four tests: Rayleigh test (Watson and Williams, 1956), Kuiper test and Rao spacing test (Batschelet, 1981; Upton and Fingleton, 1989; Mardia and Jupp, 1999) and Watson U^2 test (Watson, 1961). Results for the Watson U^2 test are shown in Supplementary Table S4. We also performed these tests at a significance level of $\alpha = 0.05$.

Comparing the mean direction between datasets

We were also looking for differences between the datasets of angles. Therefore, we performed tests to compare the mean directions.

In order to compare mean directions between several datasets that fit the vM distribution, we used the Watson-Williams test (Watson and Williams, 1956). We used the Watson nonparametric test for pairwise comparisons (Watson, 1983).

For datasets that fit the JP distribution, we used the Watson nonparametric test (Watson, 1983) for both comparisons of mean directions between several datasets and pairwise comparisons.

We used a significance level of $\alpha = 0.05$ for all the comparison of mean directions tests.

Test-based diagrams

In order to easily visualize the results of the Watson nonparametric pairwise comparison tests, we built a graph (Fig. 1F) where each node represents a dataset and two nodes that are not statistically significantly different are connected by an edge.

This kind of graph has been used before in statistical tests to compare branching angles in cells from different cortical areas (Bielza et al., 2014).

Software

Statistical analysis was performed with R Project for Statistical Computing (<https://www.r-project.org>, RRID: nif-0000-10474), and we used circular statistics in the R package (Pewsey et al., 2013; R Core Team, 2014).

RESULTS

We analyzed the branching angles of basal dendrites from 288 pyramidal neurons across layers (II, III, IV, Va, Vb, VI) of the S1HL cortex of P14 rats (Fig. 1A–C). The images of the 288 reconstructed cells organized by layers are available as supplementary material in Rojo et al. (2016).

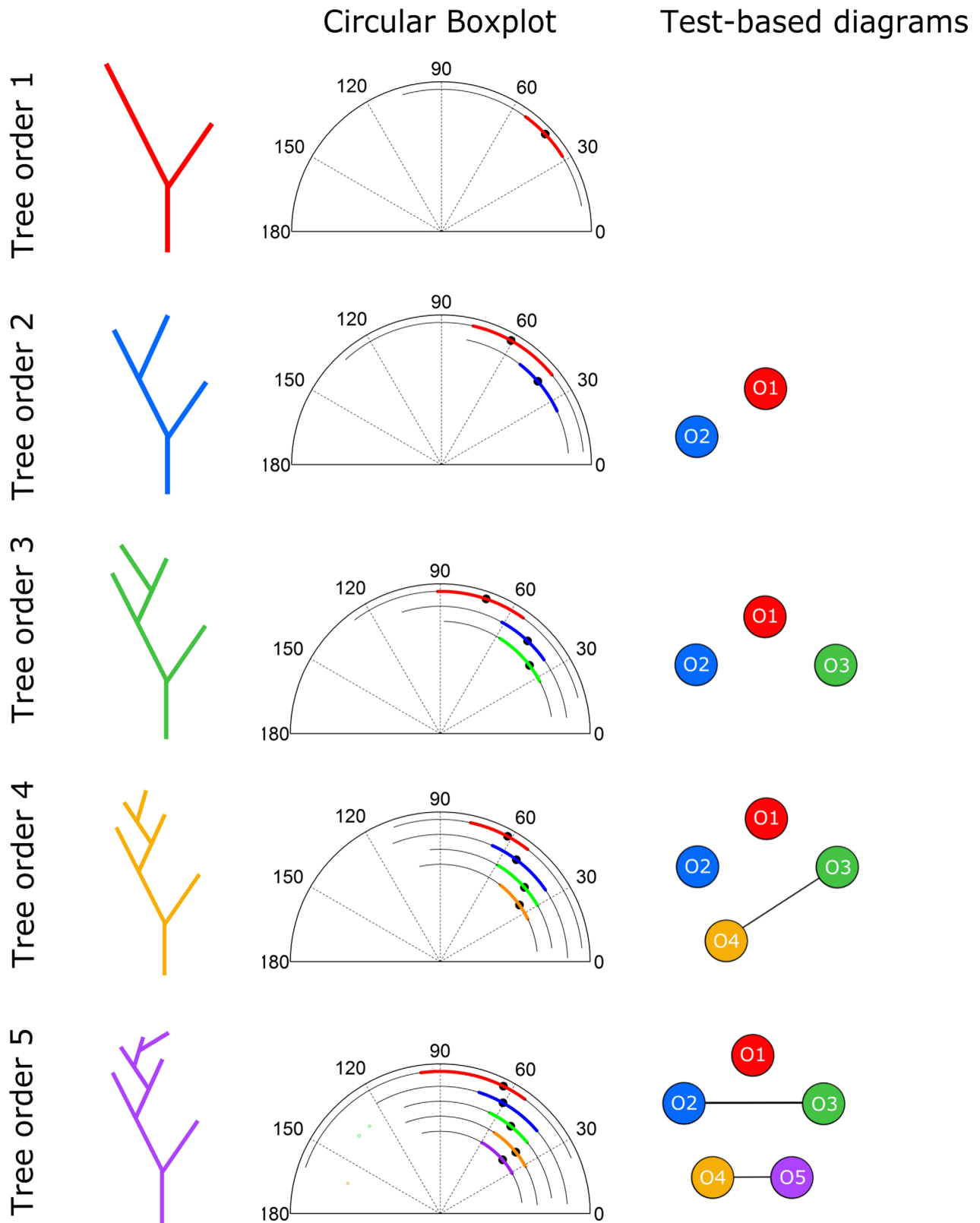


Figure 2. Left column: Diagram showing different dendritic arbors of varying complexity (different dendritic trees were grouped according to their maximum branch order). Therefore, arbors with only the first bifurcation (O1) would be denoted “T1” arbors, arbors with a maximum branching order equal to 2 as “T2”, etc. Middle column: Circular boxplots showing comparisons of angles of different branch orders from dendritic trees of same maximum tree order from layer II. Right column: The test-based diagrams corresponding to the pairwise statistical test results from Supplementary Tables S7–S8 are illustrated next to each graph. See Supplementary Figure 3 for the remaining layers.

A visual inspection of the rose diagram and the circular histogram (Fig. 1D and Supplementary Fig. 1) revealed that the distribution of the angles were unimodal and symmetric around the mean in all branch orders. The goodness-of-fit test to a vM distribution revealed that this distribution was not good enough to model the branching angles of the same order (Supplementary Table S2), where 14 out of 30 cases were rejected. We searched further for another distribution and found that the JP distribution, a broader three-parameter family of symmetric circular distributions, was appropriate for modeling these angles (Supplementary Table S4), where only 2 out of 30 cases were rejected. There is a visually appreciable fitting improvement of the JP distribution over the vM distribution (Supplementary Fig. 1).

The distribution of the angles was further analyzed using the maximum tree order. In this case, the distribution was again found to be unimodal and symmetric around the mean (Supplementary Fig. 7). The goodness-of-fit test to a vM distribution revealed that this distribution was appropriate for modeling angles of same maximum tree order (Supplementary Table S3).

Angles of different branch order

We used circular boxplots (see Materials and Methods for further details) to compare angles of a different branch order in different layers. We observed that the angles tend to decrease as the branch order increases in every layer (Fig. 1E and Supplementary Fig. 2). We also found that the CIQR is the widest at O1 and subsequent orders get narrower.

The results of the statistical tests (Supplementary Tables S5–S6) are illustrated in the test-based diagrams (Fig. 1F and Supplementary Fig. 2). Statistically significant differences were found for the angles in the first orders, but angles for higher orders were not significantly different.

Angles of different branch order originating from dendritic trees of similar complexity

We compared angles of different branch orders within dendritic trees that were grouped by the maximum tree order of their arbors. We compared the angles from dendritic trees of the same complexity. Regarding the boxplot (Fig. 2) and the statistical test results (Supplementary Tables S7–S8) that are illustrated in the test-based diagrams, the analysis revealed even more clearly what we observed without grouping by maximum tree order: there are statistically significant differences between the angles of first orders and there are no significant differences in higher orders. Therefore, by

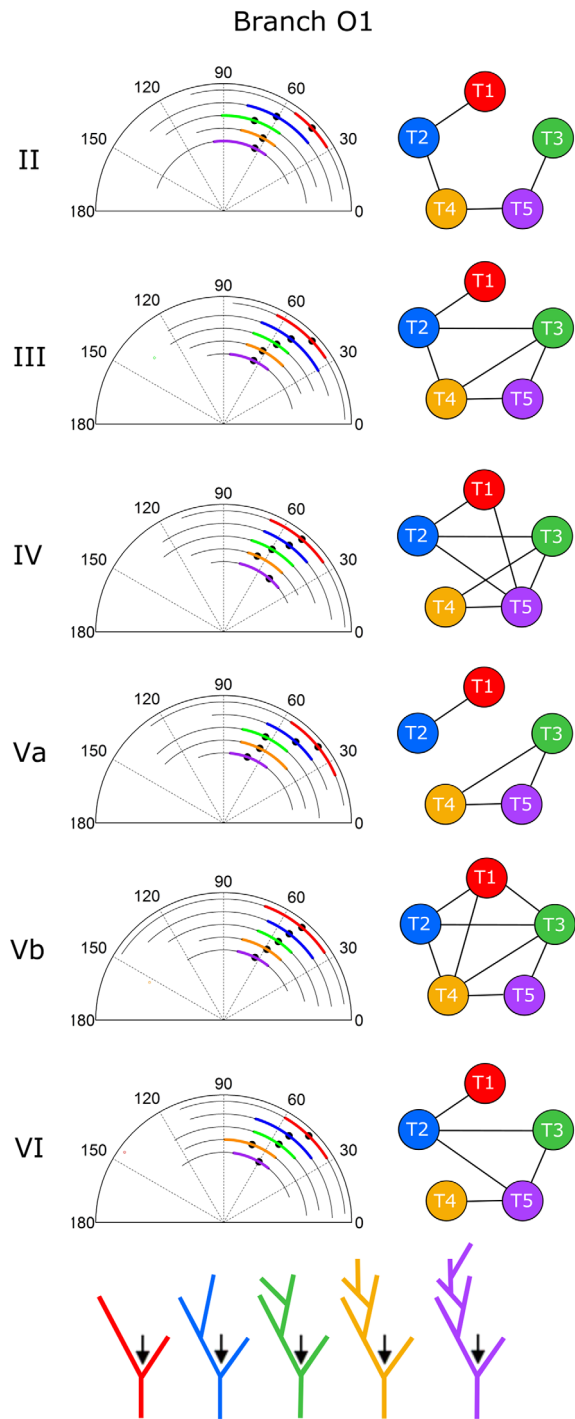


Figure 3. Circular boxplots showing comparisons of angles of branch order 1 from dendritic trees of different maximum tree order. The test-based diagrams corresponding to the pairwise statistical test results from Supplementary Tables S9–S10 are illustrated next to each graph. See Supplementary Figure 4 for the remaining branch orders.

grouping by maximum tree order, we were able to conclude that the branching angles of lower orders are wider than the branching angles of higher orders.

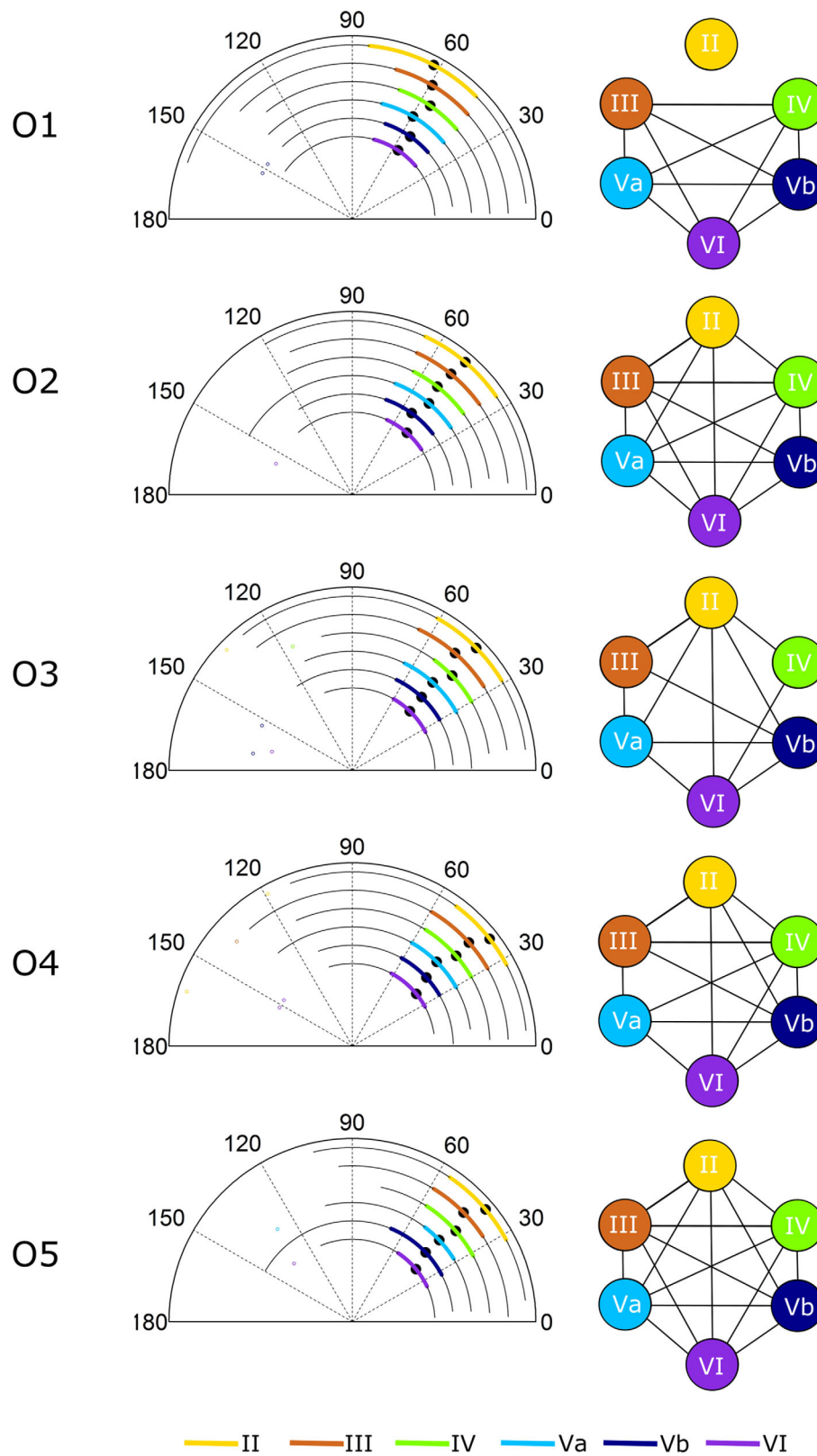


Figure 4. Circular boxplots showing comparisons of angles of same branch order in different layers. The test-based diagrams corresponding to the pairwise statistical test results from Supplementary Tables S11–S12 are illustrated next to each graph.

Angles of the same branch order originating from dendritic trees of different complexity

We compared the bifurcation angles of the same branch order that belong to trees of varying complexity. We observed in the boxplots (Fig. 3) that angles are wider for more complex arbors. This behavior is similar in all cortical layers. However, there is no statistically significant difference (Supplementary Tables S9–S10) between angles of the same branch order that belong to arbors with a maximum tree order greater than three, and the maximum tree order is equal to three in most cases.

Additionally, we compared the final branching angles from trees of varying complexity, which, from the boxplots (Supplementary Fig. 5), we found to be very similar in all cases. The statistical tests (Supplementary Tables S15–S16) reveal that there are no differences between the final angles of different branch order, and, as we observed graphically in the test-based diagrams, this behavior is the same for every layer.

Angles of different cortical layers

Finally, we compared angles between layers (II, III, IV, Va, Vb, VI). As shown in Figure 4, angles of the same branch order are similar between layers. Nevertheless, we found that the closer the layer in which the neuron is located is to the pia, the less concentrated the distribution of the angles. The statistical test results (Supplementary Tables S11–S12) illustrated in the test-based diagrams (Fig. 4) showed that there were no statistically significant differences between the angles of the same order from different layers, with the exception of layer II at O1, which did exhibit statistically significant differences. Furthermore, O1 branching angles from layer II are wider than O1 branching angles from the other layers.

We also analyzed the differences between branching angles from different layers grouped by trees of similar complexity. An example of the boxplots (Supplementary Fig. 6) showed that the distribution of the angles is again less concentrated the closer the layer is to the pia. Similarly, statistical test results (Supplementary Tables S13–S14) showed that there were no statistically significant differences between the branching angles from different layers of the same order in arbors of the same complexity (as also illustrated in the test-based diagram).

DISCUSSION

The main findings of this study are three: 1) the first bifurcation of a particular basal tree is the widest, and subsequent bifurcations become progressively narrower

in all cortical layers; 2) the final bifurcation angle of a dendritic tree is similar regardless of its complexity; and 3) angles of the same branch order are similar to each other in the different cortical layers.

We used circular distributions to model the branching angles in 3D reconstructed basal arbors. Previous studies showed that the von Mises distribution seems to be suitable for modeling the angles generated from dendritic arbor bifurcations in neurons from different cortical areas (Bielza et al., 2014). Here we reveal that the von Mises distribution is also suitable for modeling angles in neurons from different layers when grouped according to their maximum tree order, whereas angles grouped just by branch order fit the Jones-Pewsey distribution (a generic circular distribution of which the von Mises distribution is one instance).

Importantly, the results of this and a previous study regarding the geometry of pyramidal cell basal arbors in different cortical areas of adult mice (Bielza et al., 2014) are similar: the first bifurcation of a particular basal tree is the widest and subsequent bifurcations become progressively narrower in both studies. This suggests that the first orders (1 and 2) determine the space that the growing dendritic tree is to fill. In addition, the final bifurcation of a particular tree is rather similar, regardless of the maximum tree order of the arbor. Furthermore, they found, in mice, that 90% of these angles were within a range of 20–97° (per cortical area, mean angles ranged from 59–68° and concentrations ranged from 5–8). These are similar values to the results of this study (angles ranged from 10–104° per cortical layer, mean angles ranged from 41.82–64.17° and concentrations ranged from 4.71–9.62). We should stress that these rules were observed regardless of the differences in the size and complexity of the basal dendritic arbors of these cells between the cortical areas of the mice (Bielza et al., 2014) or between the cortical layers of the rats (Rojo et al., 2016). Thus, these rules seem to be a general organizational principle in the design of pyramidal cell architecture, despite the different functional specializations of cortical layers and areas and species.

In the mouse cerebral cortex, however, it was observed that the mean final branch order angle was remarkably different in the seven examined cortical regions (Bielza et al., 2014). In general, cortical regions with larger dendritic trees had smaller final bifurcation angles. However, no significant differences were found between the branch order angles of pyramidal cells across layers of the juvenile rat somatosensory cortex despite the systematic variation in the basal dendritic pattern (Rojo et al., 2016). Briefly, cells became larger and progressively more complex in their branching

structure from superficial to deeper layers, except for those in layer IV, which were the simplest cells. Taken together, these results suggest that the final branch order angle may constitute an area-specific feature. Further studies of the different dendritic compartments (e.g., apical arbor), cortical regions, and species would need to be performed to make such a generalization. In addition, since we examined juvenile rats, it would be interesting to analyze if branching angle structure in the adult rat cortex remains the same as in the juvenile rats in order to make species comparisons.

Clearly, it is of critical importance to determine these rules since general principles of cortical synaptic connections also exist. Therefore, the integration of the morphological rules of pyramidal cells with the principles of their synaptic connection is fundamental in order to gain a better understanding of the design of cortical circuits. For instance, most excitatory, glutamatergic synapses on pyramidal neurons are established with their dendritic spines, whereas most inhibitory GABAergic synapses are established mainly in the dendritic shafts, but the vast majority of synapses are established on the dendritic spines (reviewed in DeFelipe and Fariñas, 1992), the length of which is typically $<2 \mu\text{m}$, (e.g., Ballesteros-Yáñez et al., 2006; Benavides-Piccione et al., 2012). Therefore, differences in the complexity, dendritic length, and dendritic spine density of the dendritic tree between layers reflect differences in the total number of excitatory and inhibitory synapses in the pyramidal neurons. However, the fact that no significant differences were found between the branch order angles of pyramidal cells across layers suggests that there is some predictability in the synaptic connections of pyramidal cells in all cortical layers that is independent of the total number of synaptic inputs. Thus, the variations in pyramidal cell structure indicate that the cortical circuits in which these cells participate are likely to be characterized by different functional capabilities (integration of excitatory and inhibitory synapses). However, we do not know whether the branch angles have a significant direct impact on signal processing per se. Computational simulations performed by Ferrante et al. (2013) have shown that minor changes in dendritic branch-point morphology of CA1 apical trees of pyramidal cells can lead to major modifications in the integrative properties of oblique dendrites. In this regard, further computational modeling studies could also contribute towards attempts to predict the biophysical consequences of varying branch angles of the basal dendrites from the first (the wider) to the subsequent bifurcations, which become progressively narrower. A further point to note is the fact that the structure between the branch order angles of pyramidal

cells is unchanged across layers, which supports the idea that the factors that intrinsically regulate dendritic branching development are probably related to the rules that determine the general connectivity of the pyramidal cell. More specifically, our results seem to indicate the existence of spatial synaptic connectivity rules of pyramidal neurons that are constrained by the relatively narrow value windows of the bifurcation angles. Finally, the computational attributes of pyramidal cells depend not only on their basal dendritic arbors, but also on the structure of their apical dendrites. Thus, we are planning to address some of these questions by analyzing the apical arbor in the near future. Additional studies in other species/cortical areas and ages are necessary to further elucidate the generally applicable and specific rules governing the geometry of cortical pyramidal cells.

CONFLICT OF INTEREST

The authors declare that there are no conflicts of interest.

ROLE OF AUTHORS

All authors had full access to all the data in the study and took responsibility for the data integrity and the data analysis rigor. Study concept and design: IL, CB, PL, RB, JD. Acquisition of data: AK, CR, RB, JD. Analysis and interpretation of data: IL, CB, PL, RB, JD. Drafting of the article: IL, RB. Critical revision of the article for important intellectual content: CB, PL, RB, JD. Statistical analysis: IL, CB, PL. Obtained funding: IL, CB, PL, RB, JD. Administrative, technical, and material support: CB, PL, RB, JD. Study supervision: CB, PL, RB, JD.

LITERATURE CITED

- Abuzaid AH, Mohamed IB, Hussin AG. 2012. Boxplot for circular variables. *J Comput Stat* 27:381–392.
- Ballesteros-Yáñez I, Benavides-Piccione R, Elston G, Yuste R, DeFelipe J. 2006. Density and morphology of dendritic spines in mouse neocortex. *Neuroscience* 138:403–409.
- Batschelet E. 1981. *Circular statistics in biology*. London: Academic Press.
- Benavides-Piccione R, Hamzei-Sichani F, Ballesteros-Yáñez I, DeFelipe J, Yuste R. 2006. Dendritic size of pyramidal neurons differs among mouse cortical regions. *Cereb Cortex* 16:990–1001.
- Benavides-Piccione R, Fernaud-Espinosa I, Robles V, Yuste R, DeFelipe J. 2012. Age-based comparison of human dendritic spine structure using complete three-dimensional reconstructions. *Cereb Cortex* 23:1798–1810.
- Bielza C, Benavides-Piccione R, López-Cruz P, Larrañaga P, DeFelipe J. 2014. Branching angles of pyramidal cell dendrites follow common geometrical design principles in different cortical areas. *Sci Rep* 4:5909.
- Cuntz H, Borst A, Segev I. 2008. Optimization principles of dendritic structure. *Theor Biol Med Model* 4:21.

- Cuntz H, Forstner F, Vorst AH, M. 2010. One rule to grow them all: A general theory of neuronal branching and its practical application. *PLoS Comput Biol* 6.
- Cuntz H, Mathy A, Häusser M. 2012. A scaling law derived from optimal dendritic wiring. *Proc Natl Acad Sci U S A* 109:11014–11018.
- DeFelipe J. 2015. The dendritic spine story: an intriguing process of discovery. *Front Neuroanat* 9:14.
- DeFelipe J, Fariñas I. 1992. The pyramidal neuron of the cerebral cortex: Morphological and chemical characteristics of the synaptic inputs. *Prog Neurobiol* 39:563–607.
- Elston GN. 2003. Cortex, cognition and the cell: new insights into the pyramidal neuron and prefrontal function. *Cereb Cortex* 13:1124–1138.
- Elston GN, Benavides-Piccione R, DeFelipe J. 2001. The pyramidal cell in cognition: a comparative study in human and monkey. *J Neurosci* 21:RC163.
- Ferrante M, Migliore M, Ascoli GA. 2013. Functional impact of dendritic branch-point morphology. *J Neurosci* 33:2156–2165.
- Fisher NI. 1993. *Statistical analysis of circular data*. London: Cambridge University Press.
- Gradshteyn IS, Ryzhik IM. 1994. *Table of integrals, series, and products* (5th ed.). New York: Academic Press. p 58.
- Jacobs B, Schall M, Prather M, Kapler L, Driscoll L, Baca S, Jacobs J, Ford K, Wainwright M, Trembl M. 2001. Regional dendritic and spine variation in human cerebral cortex: a quantitative study. *Cereb Cortex* 11:558–571.
- Jammalamadaka SR, SenGupta A. 2001. *Topics in circular statistics*. Hackensack, NJ: World Scientific Publishing.
- Jones MC, Pewsey A. 2005. A family of symmetric distributions on the circle. *J Am Stat Assoc* 100:1422–1428.
- Kabaso D, Coskren PJ, Henry BI, Hof PR, Wearne SL. 2009. The electronic structure of pyramidal neurons contributing to prefrontal cortical circuits in macaque monkeys is significantly altered in aging. *Cereb Cortex* 19:2248–2268.
- Kim Y, Sinclair R, Chindapol N, Kaandorp JA, De Schutter E. 2012. Geometric theory predicts bifurcations in minimal wiring cost trees in biology are flat. *PLoS Comput Biol* 8:e1002474.
- Larkman AU. 1991. Dendritic morphology of pyramidal neurons in the visual cortex of the rat. I. Branching patterns. *J Comp Neurol* 306:307–319.
- Lockhart RA, Stephens MA. 1985. Tests of fit for the von Mises distribution. *Biometrika* 72:647–652.
- López-Cruz PL, Bielza C, Larrañaga P, Benavides-Piccione R, DeFelipe J. 2011. Models and simulation of 3D neuronal dendritic trees using Bayesian networks. *Neuroinformatics* 9:347–369.
- Mardia KB, Jupp PE. 1999. *Directional statistics*. London: Wiley.
- Oberlander M, de Kock CP, Bruno RM, Ramirez A, Meyer HS, Dercksen VJ, Helmstaedter M, Sakmann B. 2012. Cell type-specific three-dimensional structure of thalamocortical circuits in a column of rat vibrissa cortex. *Cereb Cortex* 22:2375–2391.
- Petanjek Z, Judas M, Kostovic I, Uylings HB. 2008. Lifespan alterations of basal dendritic trees of pyramidal neurons in the human prefrontal cortex: a layer-specific pattern. *Cereb Cortex* 18:915–929.
- Pewsey A, Neuhäuser M, Ruxton AD. 2013. *Circular statistics in R*. Oxford, UK: Oxford University Press.
- Rojo C, Leguey I, Kastanauskaite A, Bielza C, Larrañaga P, DeFelipe J, Benavides-Piccione R. 2016. Laminar differences in dendritic structure of pyramidal neurons in the juvenile rat somatosensory cortex. *Cereb Cortex* [Epub ahead of print].
- Samsonovich AV, Ascoli GA. 2003. Statistical morphological analysis of hippocampal principal neurons indicates cell-specific repulsion of dendrites from their own cell. *J Neurosci Res* 71:173–187.
- Spruston N. 2008. Pyramidal neurons: dendritic structure and synaptic integration. *Nat Rev Neurosci* 9:206–221.
- Stuart G, Spruston N. 2015. Dendritic integration: 60 years of progress. *Nat Neurosci* 18:1713–1721.
- Team RC. 2014. *R: A Language and Environment for Statistical Computing*. Vienna, Austria: R Foundation for Statistical Computing.
- Upton GJG, Fingleton B. 1989. *Spatial data analysis by example. Volume 2: Categorical and directional data*. New York: John Wiley & Sons.
- van Pelt J, Uylings HB. 2011. The flatness of bifurcations in 3D dendritic trees: an optimal design. *Front Comput Neurosci* 5:54.
- von Mises R. 1918. Über die “Ganzzahligkeit” der Atomgewichte and verwandte Fragen. *Physik Zeit* 19:490–500.
- Watson GS. 1961. Goodness-of-fit test on a circle. *Biometrika* 48:109–114.
- Watson GS. 1983. *Statistics on spheres*. New York: John Wiley & Sons.
- Watson GS, Williams E. 1956. On the construction of significance test on the circle and the sphere. *Biometrika* 43:344–352.
- Wen Q, Chklovskii DB. 2008. A cost-benefit analysis of neuronal morphology. *J Neurophysiol* 99:2320–2328.
- Wen Q, Stepanyants A, Elston GN, Grosberg AY, Chklovskii DB. 2009. Maximization of the connectivity repertoire as a statistical principle governing the shapes of dendritic arbors. *Proc Natl Acad Sci U S A* 106:12536–12541.
- Yuste R. 2010. *Dendritic spines*. Cambridge, UK: MIT Press.
- Zwillinger D. 1997. *Handbook of differential equations*, 3rd ed. Houston, TX: Gulf Professional Publishing.